Mon. Not. R. Astron. Soc. **000**, 000–000 (0000) Printed 24 July 2014 (MN LATEX style file v2.2)

Fractional anisotropy as an optimal tracer of cosmic voids

Sebastian Bustamante ⋆[1] Jaime E. Forero-Romero[2]

[1] *Instituto de Física - FCEN, Universidad de Antioquia, Calle 67 No. 53-108, Medellín, Colombia*
[2] *Departamento de Física, Universidad de los Andes, Cra. 1 No. 18A-10, Edificio Ip, Bogotá, Colombia*

24 July 2014

ABSTRACT

Key words: Cosmology: large-scale Structure of Universe, galaxies: star formation - line: formation

1 INTRODUCTION

Since voids where discovered in the first compiled galaxy surveys (Chincarini & Rood 1975; Gregory & Thompson 1978; Einasto et al. 1980a,b; Kirshner et al. 1981, 1987), they have been identified, along with the filamentary and hierarchically clustered nature of the cosmic web, as one of the most striking features of the Megaparsec universe (Bond et al. 1996). Nevertheless, due to the large volume extension of void regions ($\sim 5-10$ Mpch^{-1}), statistically significant catalogues of voids (Pan et al. 2012; Sutter et al. 2012; Nadathur & Hotchkiss 2014) only have become available after modern large galaxy surveys like the two-degree field Galaxy Survey (Colless et al. 2001, 2003) and the Sloan Digital Sky Survey (York et al. 2000; Abazajian et al. 2003), thereby triggering a plethora of more refined observational and statistical studies of voids throughout the last decade (Hoyle & Vogeley 2004; Croton & et al. 2004; Rojas et al. 2005; Ceccarelli et al. 2006; Patiri et al. 2006; Tikhonov 2006; Patiri et al. 2006; Tikhonov 2007; von Benda-Beckmann & Müller 2008; Foster & Nelson 2009; Ceccarelli et al. 2013; Sutter et al. 2014)

On the theoretical side, early descriptions of the evolution of the large-scale universe, leaded by the seminal work of Zel'dovich (1970), are highly consistent with the cosmic web picture, where planar pancake-like regions of matter enclose enormous sub-dense voids and are bordered, in turn, by thin filaments and high-density clumpy knots. First theoretical models for describing formation, dynamics and properties of voids (Hoffman & Shaham 1982; Icke 1984; Bertschinger 1985; Blumenthal et al. 1992) were quickly complemented and extended by first numerical studies based on simulations (Martel & Wasserman 1990; Regos & Geller 1991; van de Weygaert & van Kampen 1993; Dubinski et al. 1993). This tendency of using numerical results from N-body simulations, fuelled by last generation computing systems, has become increasingly common in the two last decades as a powerful analysis tool in studies of cosmic voids (Gottlöber et al. 2003).

2 THE SIMULATION

We use here an unconstrained cosmological simulation, the Bolshoi simulation, to identify the possible large scale environment and cosmological voids.

The Bolshoi simulation follows the non-linear evolution of a dark matter density field on a cubic volume of size $250h^{-1}$Mpc sampled with 2048^3 particles. The cosmological parameters in the simulation are $\Omega_{\rm m} = 0.27$, $\Omega_\Lambda = 0.73$, $h = 0.70$, $n = 0.95$ and $\sigma_8 = 0.82$ for the matter density, cosmological constant, dimensionless Hubble parameter, spectral index of primordial density perturbations and normalization for the power spectrum. The mass of each particle in the simulation is $m_{\rm p} = 1.4 \times 10^8 h^{-1} {\rm M}_\odot$. We identify catalogues of halos through the Bound Density Maximum algorithm.

3 ALGORITHMS TO QUANTIFY THE COSMIC WEB

3.1 The tidal web (T-web)

The first algorithm we use to identify the cosmic web is based upon the diagonalization of the tidal tensor, defined as the Hessian of a normalized gravitational potential

$$T_{\alpha\beta} = \frac{\partial^2 \phi}{\partial x_\alpha \partial x_\beta} \tag{1}$$

where the physical gravitational potential has been rescaled by a factor $4\pi G\bar{\rho}$ in such a way that ϕ satisfies the following equation

$$\nabla^2 \phi = \delta, \tag{2}$$

⋆ sbustama@pegasus.udea.edu.co

where $\bar{\rho}$ is the average density in the Universe, G is the gravitational constant and δ is the dimensionless matter overdensity.

3.2 The velocity web (V-web)

We also use a kinematical method to define the cosmic-web environment in the simulation. The method has been thoroughly described in XXX and applied to study the shape and spin alignment in the Bolshoi simulation here XX. We refer the reader to these papers to find a detailed description of the algorithm, its limitations and capabilities. Here we summarize the most relevant points for the discussion.

The V-web method for environment finding is based on the local shear tensor calculated from the smoothed DM velocity field in the simulation. The central quantity is the following dimensionless quantity

$$\Sigma_{\alpha\beta} = -\frac{1}{2H_0}\left(\frac{\partial v_\alpha}{\partial x_\beta} + \frac{\partial v_\beta}{\partial x_\alpha}\right) \quad (3)$$

where v_α and x_α represent the α component of the comoving velocity and position, respectively. $\Sigma_{\alpha\beta}$ can be represented by a 3×3 symmetric matrix with real values, that ensures that is possible to diagonalize and obtain three real eigenvalues $\lambda_1 > \lambda_2 > \lambda_3$ whose sum (the trace of $\Sigma_{\alpha\beta}$) is proportional to the divergence of the local velocity field smoothed on the physical scale $\mathcal{R}$.

The relative strength of the three eigenvalues with respect to a threshold value λ_{th} allows for the local classification of the matter distribution into four web types: voids, sheets, filaments and peaks, which correspond to regions with 3, 2, 1 or 0 eigenvalues with values larger than λ_{th}. Below we shall discuss a novel approach to define an adequate threshold value based on the visual impression of void regions, furthermore we study other possible values based on other visual features of the cosmic web.

4 FINDING BULK VOIDS

4.1 Fractional anisotropy as tracer of voids

According to the recent growing interest in studying galaxy formation in low-density regions as cosmological tests, classifying void regions is becoming an important task in cosmology. Most of those classification schemes for voids in cosmological simulations are based upon the density field, setting a cut off value below which some region becomes a void **[references]**. Some more advanced classification schemes are based on Voronoi tessellations applied over the tracer particles of the simulation in order to compute the density field. Then, through a watershed transform, a hierarchy of void regions are found **[references, ZOBOV algorithm]**.

As has been established **[references]**, both web schemes presented in the previous section (V-web and T-web) for classifying the cosmic web present many advantages compared with classification schemes based completely upon the density field, e.g. a more robust description of the dynamic a kinematic of the cosmic web, a more reliable quantification of the visual impression, among others. With the aim of exploiting all of these advantages, we propose here a novel approach to classify voids in cosmological simulations based entirely on the web schemes.

The original version of the T-web scheme **[reference, Hahn]** was not successful at reproducing the visual impression of the cosmic web, however, with the introduction of a threshold parameter **[reference, Forero-Romero]**, this scheme, and even the V-web **[reference, Hoffman]**, improved enormously. As this free parameter controls the visual impression provided by each scheme, phenomenons like percolation depends on it as well. Although percolation is one of the key features of the structure of void regions, indicating how voids are merged among them, and how they permeate all the cosmic web, our primal interest here is studying properties of single voids. Nevertheless, in the next section we shall analyse briefly the percolation phenomenon for both web schemes.

In order to deal with percolation of voids in our classification scheme, we introduce the fractional anisotropy as defined in **[reference, Libeskind]**.

$$FA = \frac{1}{\sqrt{3}}\sqrt{\frac{(\lambda_1-\lambda_3)^2 + (\lambda_2-\lambda_3)^2 + (\lambda_1-\lambda_2)^2}{\lambda_1^2+\lambda_2^2+\lambda_3^2}} \quad (4)$$

where the eigenvalues are taken from any of the two web schemes. This index, such as it is defined, allows quantifying the local anisotropy degree of the cosmological environment, where $FA = 0$ corresponds to highly isotropic regions and $FA = 1$ anisotropic ones.

In the figure 5 we calculate the FA field over the simulation for both web schemes. The first interesting feature of this figure is the degeneration presented for knots and central regions of voids, where both of them exhibit low to middle values of the FA, indicating a high isotropy regarding the physical properties quantified by each web scheme, i.e. the density field for the T-web and the peculiar velocity for the V-web. For the T-web, the FA field near to knots presents a very narrow distribution around a local minimum, whereas for the V-web such distribution is more spread out. This can be explained appealing to the low fluctuations of the density field compared with the peculiar velocity in highly non-linear regions like knots. For more linear regions like voids, the behaviour of the FA field is quite similar between both schemes, what is consistent with the equivalence of the T-web and the V-web in the linear regime **[reference, Hoffman]**.

According to the classification scheme adopted for the cosmological environment, voids are regions where $\lambda_3 \leqslant \lambda_2 \leqslant \lambda_1 \leqslant \lambda_{th}$. This implies that the boundaries of void regions are controlled completely by the λ_1 eigenvalue of the web scheme and the threshold value. Therefore, as we increase the threshold value λ_{th}, all voids grow up progressively through contours of the λ_1 field until certain critical value where they are so large that the visual impression is no longer reproduced. Our objective here is to find a reliable quantity that allows to trace the geometry of void regions as classified by each web scheme. In the figure 2 we calculate the distributions of the fractional anisotropy index and the density field regarding the λ_1 eigenvalue for both web schemes over all the cells of the simulation. Thick lines correspond to the median of the distributions, whereas coloured regions correspond to 50% of the sample, delimited by quartiles Q_1 and Q_3.

The first important conclusion is regarding the distribution of the FA index, where there is an almost perfect correlation with the λ_1 eigenvalue for low values of it. This result can be interpreted as an one-dimensional tomography of void regions, where low λ_1 values are associated to the central regions of voids, these being the most isotropic structures found, with FA values close to 0. As we increase the λ_1 value, corresponding to progressively outer layers of void regions or less isotropic voids, the FA index increases as well, maintaining a very reliable correlation approximately until $FA = 0.95$. This limit value of the FA can be traduced in terms of an optimal λ_{th} , where we obtain $\lambda^V_{opt} = 0.175$ for the V-web scheme and $\lambda^T_{opt} = 0.265$ for the T-web scheme, both values consistent with optimal thresholds normally taken in previous works **[references]**. Due to the definition of the fractional anisotropy index, it presents the highest values for filaments and very flat sheets, i.e. $FA \lesssim 1$. Therefore, if we extend the λ_{th} value beyond the optimal FA limit, such that the outer regions of voids becomes highly anisotropic, it would imply that voids are invading filaments and sheets, so the optimal λ_{th} value is a limit value up to which we can have void regions. For other type of environment such as sheets, filaments and knots, the λ_1 eigenvalue does not control their spatial boundaries, so the correlation with the FA index is no longer valid beyond the threshold values, furthermore the larger dispersion of the FA distribution also indicates that contours of the FA field are no longer corresponding to contours of the λ_1 field. Nevertheless, for high λ_1 values, i.e. $\lambda_1 > 1.0$, the median value of the FA index decreases to lower values, indicating the presence of isotropic knots. All of this allows us to conclude that the distribution of the FA with respect to the λ_1 eigenvalue is not only an one-dimensional tomography of voids, but also a sort of one-dimensional projection of the global structure of the cosmic web, starting in highly isotropic central voids, passing through very anisotropic sheets and filaments, until isotropic knot regions.

For the distribution of the density with respect to the λ_1 eigenvalue, it can be appreciated an analogous behaviour, where central regions of voids present the most under-dense values of the overall cosmic web. For outer layers of voids, the density field grows progressively until sheets and filaments are reached. However, the dispersion in the distributions indicates that the geometry of voids as quantified by both web schemes is not compatible with the density field, i.e. contours of the λ_1 eigenvalue do not coincide with contours of the density field. Then, the density is not a reliable quantity to be used as tracer of our voids. Furthermore, another advantage of using the FA index instead of the density is the non-monotonous behaviour of the FA median value, with a local maxima that allows to identify properly the boundaries of voids.

4.2 Identifying void regions through web schemes

Resuming our endeavour at identifying voids in cosmological simulations, previous techniques based on web classification schemes usually perform a FOF-like algorithm over cells previously marked as voids according to some established criteria in order to construct bulk void regions **[references]**. Although this method has some success at classifying voids, percolation is completely inevitable, where the only way to reduce it is artificially decreasing the global volume fraction of void regions such that they do not merge significantly each other.

Once has been determined the reliability of the FA index for tracing the geometry of voids, our novel proposal here is rather using the FA field for classifying void regions. As was concluded in the previous subsection, the geometry of voids is completely traced by contours of the FA field, where central parts of voids and high density knot regions exhibit particularly low values of the FA index. Therefore, through a watershed transform all voids are classified, where each single void region corresponds to the basin of a local minimum of the FA field, where those local minimums are restricted to be embedded into a type-void cell in order to avoid degeneracy with knots.

5 PROPERTIES OF VOIDS

Once defined our method to classify bulk voids based upon web classification schemes of the cosmic web, we proceed to analyse some physical properties in order to compare their consistency with the geometry of voids as quantified by our method and by density-based schemes. Next, through the reduced inertia tensor we quantify the shape distribution of voids. Finally, we compute numerical radial profiles of density and peculiar velocity of bulk voids.

5.1 Statistics of halos in voids

One of the main challenges in observational void finding is the discrete nature of galaxy surveys

we calculate contours of discrete fields like the median mass and the local number of local dark matter halos and

, like the inertia values, the density and peculiar velocities profiles as calculated over the grid and profiles of number of halos.

5.2 Shape of voids

Quantifying the shape of voids is gaining importance due to cosmological tests such as the Alcock-Paczynski test **[Sutter et al 2012]**, so we compute here the reduced inertia tensor through the next expression in order to determine shape distributions of bulk voids.

$$\tau_{ij} = \sum_l \frac{x_{l,i} x_{l,j}}{R_l^2} \tag{5}$$

where l is an index associated to each cell of the current region, i and j indexes run over each spatial direction and finally R_l is defined as $R_l^2 = x_{l,1}^2 + x_{l,2}^2 + x_{l,3}^2$. All positions are measured from the respective geometric center of each void.

The eigenvalues of the reduced inertia tensor, i.e. the principal moments of inertia, are used to quantify the shape of each bulk void. They are denoted as τ_1, τ_2 and τ_3 such that $\tau_1 \leqslant \tau_2 \leqslant \tau_3$. In Figure **??** we show the computed distributions for τ_1/τ_2 and τ_2/τ_3 for voids larger than 8 cells in order to avoid statistic fluctuations due to small regions. We rather calculate histograms for these ratio quantities instead of each single value in order to avoid using an arbitrary

normalization. For both schemes, it can be noticed that the shape distribution is completely spread out, thereby indicating a non-preferred geometry of void regions, which is in agreement with the well established high anisotropy of matter flows associated to this type of region.

For a better quantification, we also perform a classification of the shape of voids by setting a threshold in the analysed ratio quantities. An anisotropic or tri-axial shape correspond to voids where $\tau_1/\tau_2 < 0.7$ and $\tau_2/\tau_3 < 0.7$, where there is not any symmetry among the principal directions. We find about $57.2\% \sim 61.0\%$ of total voids consistent with this shape, for the T-web and V-web respectively. A pancake or quasi-oblate shape is associated to voids where $\tau_1/\tau_2 < 0.7$ and $\tau_2/\tau_3 > 0.7$. We found $13.1\% \sim 17.9\%$ of consistent voids. Filamentary or quasi-prolate voids satisfy $\tau_1/\tau_2 > 0.7$ and $\tau_2/\tau_3 < 0.7$, with $25.4\% \sim 18.1\%$ of all voids. Finally, isotropic or quasi-spheric voids are found when $\tau_1/\tau_2 > 0.7$ and $\tau_2/\tau_3 > 0.7$, with $4.2\% \sim 3.1\%$ of total voids compatible with this shape. The threshold value of 0.7 adopted here for the ratios of the moments of inertia is just for illustrative purposes, where such distinction is rather fuzzy and continuous. However, the previous analysis allows us to conclude that voids are quite asymmetric structures.

5.3 Density profile of voids

Describing the density profiles of voids is quite important in order to compare and match simulation with observational surveys, allowing possible constrains for different cosmology models **[Hamaous, et.al 2014]**. Here, and taking into account the previous results, we rather use an ellipsoidal approximation to describe and fit the shape of bulk voids, so we use the next ellipsoidal radial coordinate to describe density profiles.

$$r^2 = \frac{x^2}{\tau_1^2} + \frac{y^2}{\tau_2^2} + \frac{z^2}{\tau_3^2}, \quad 0 \leqslant r \leqslant 1 \tag{6}$$

where we take the principal moments of inertia $\{\tau_i\}$ as the lengths of the principal axes of the ellipsoid and each one of the cartesian coordinates as measured in the rotated frame of each void.

We use the same analytic density profile that **[Hamaous, et.al 2014]** to fit the numerical density profiles of our voids.

$$\delta_v(r) = \delta_c \frac{1 - (r/r_s)^\alpha}{1 + (r/r_v)^\beta} \tag{7}$$

6 CONCLUSIONS

ACKNOWLEDGMENTS

REFERENCES

Abazajian K., et al. (the SDSS Collaboration) 2003, AJ, 126, 2081

Bertschinger E., 1985, ApJS, 58, 1

Blumenthal G. R., da Costa L. N., Goldwirth D. S., Lecar M., Piran T., 1992, ApJ, 388, 234

Bond J. R., Kofman L., Pogosyan D., 1996, Nature, 380, 603

Ceccarelli L., Padilla N. D., Valotto C., Lambas D. G., 2006, MNRAS, 373, 1440

Ceccarelli L., Paz D., Lares M., Padilla N., Lambas D. G., 2013, MNRAS, 434, 1435

Chincarini G., Rood H. J., 1975, Nature, 257, 294

Colless M., et al. (the 2dFGRS Team), 2001, MNRAS, 328, 1039

Colless M., et al. (the 2dFGRS Team), 2003, VizieR Online Data Catalog, 7226

Croton D. J., et al. 2004, MNRAS, 352, 828

Dubinski J., da Costa L. N., Goldwirth D. S., Lecar M., Piran T., 1993, ApJ, 410, 458

Einasto J., Joeveer M., Saar E., 1980a, MNRAS, 193, 353

Einasto J., Joeveer M., Saar E., 1980b, Nature, 283, 47

Foster C., Nelson L. A., 2009, ApJ, 699, 1252

Gottlöber S., Łokas E. L., Klypin A., Hoffman Y., 2003, MNRAS, 344, 715

Gregory S. A., Thompson L. A., 1978, ApJ, 222, 784

Hoffman Y., Shaham J., 1982, ApJL, 262, L23

Hoyle F., Vogeley M. S., 2004, ApJ, 607, 751

Icke V., 1984, MNRAS, 206, 1P

Kirshner R. P., Oemler Jr. A., Schechter P. L., Shectman S. A., 1981, ApJL, 248, L57

Kirshner R. P., Oemler Jr. A., Schechter P. L., Shectman S. A., 1987, ApJ, 314, 493

Martel H., Wasserman I., 1990, ApJ, 348, 1

Nadathur S., Hotchkiss S., 2014, MNRAS, 440, 1248

Pan D. C., Vogeley M. S., Hoyle F., Choi Y.-Y., Park C., 2012, MNRAS, 421, 926

Patiri S. G., Betancort-Rijo J., Prada F., 2006, MNRAS, 368, 1132

Patiri S. G., Prada F., Holtzman J., Klypin A., Betancort-Rijo J., 2006, MNRAS, 372, 1710

Regos E., Geller M. J., 1991, ApJ, 377, 14

Rojas R. R., Vogeley M. S., Hoyle F., Brinkmann J., 2005, ApJ, 624, 571

Sutter P. M., Lavaux G., Wandelt B. D., Weinberg D. H., 2012, ApJ, 761, 44

Sutter P. M., Lavaux G., Wandelt B. D., Weinberg D. H., Warren M. S., 2014, MNRAS, 438, 3177

Tikhonov A. V., 2006, Astronomy Letters, 32, 727

Tikhonov A. V., 2007, Astronomy Letters, 33, 499

van de Weygaert R., van Kampen E., 1993, MNRAS, 263, 481

von Benda-Beckmann A. M., Müller V., 2008, MNRAS, 384, 1189

York D. G., et al. (the SDSS Collaboration), 2000, AJ, 120, 1579

Zel'dovich Y. B., 1970, A&A, 5, 84

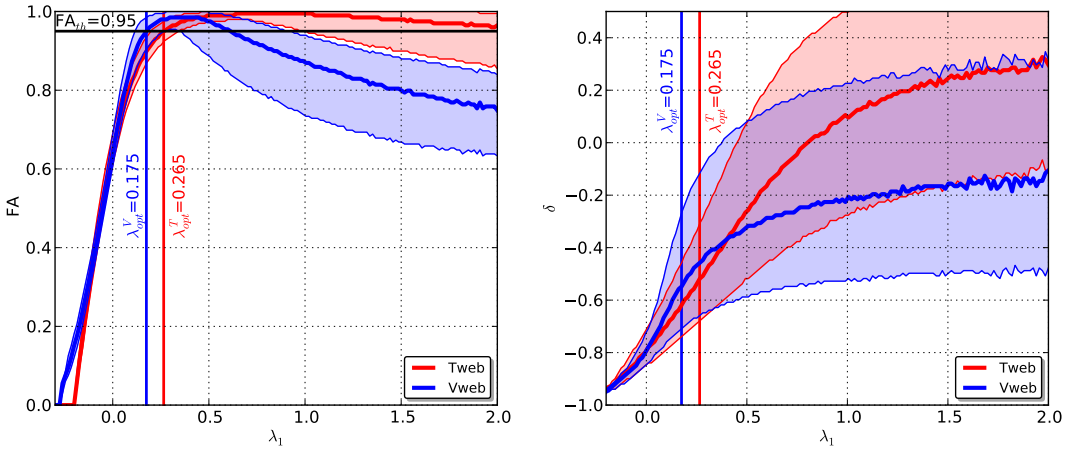

Figure 1. In this figure is shown the distribution of the fractional anisotropy (left panel) and density field (right panel) with respect to the eigenvalue λ_1 for each web scheme (T-web, red lines. V-web, blue lines) as calculated over all the cells of the grid. Thick central lines correspond to the median of the distribution and coloured regions to the 50% of the cells, delimited by quartiles Q_1 and Q_3.

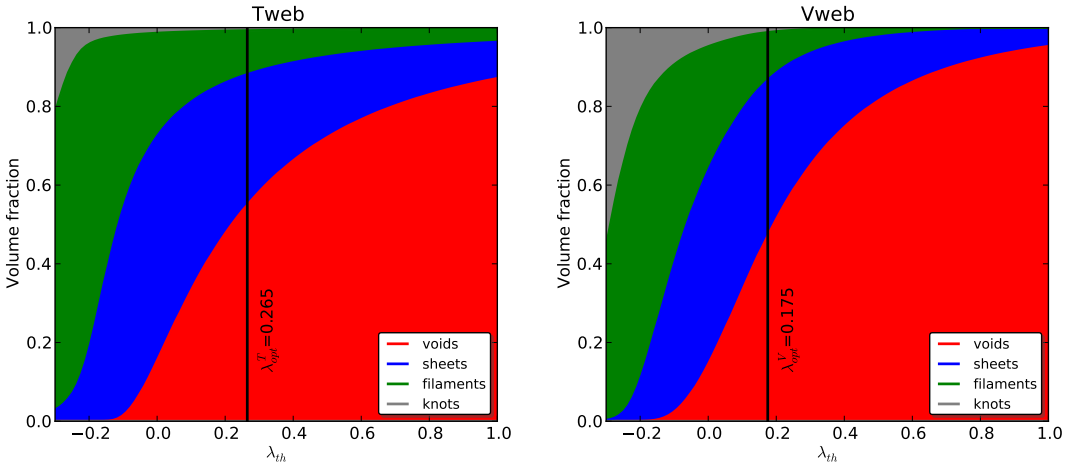

Figure 2. In this figure is shown the distribution of the fractional anisotropy (left panel) and density field (right panel) with respect to the eigenvalue λ_1 for each web scheme (T-web, red lines. V-web, blue lines) as calculated over all the cells of the grid. Thick central lines correspond to the median of the distribution and coloured regions to the 50% of the cells, delimited by quartiles Q_1 and Q_3.

volume fraction	**scheme T-web**	**V-web**	**Density**	$\delta_{\mathbf{th}}$
Voids	54.88%	47.06%	50.97%	−0.57
Sheets	33.21%	39.54%	36.38%	0.60
Filaments	11.16%	12.18%	11.67%	8.82
Knots	0.75%	1.22%	0.98%	–

Table 1: Size of each sample defined in the Bolshoi simulation and for each of the two schemes used to detect halos (FOF and BDM).

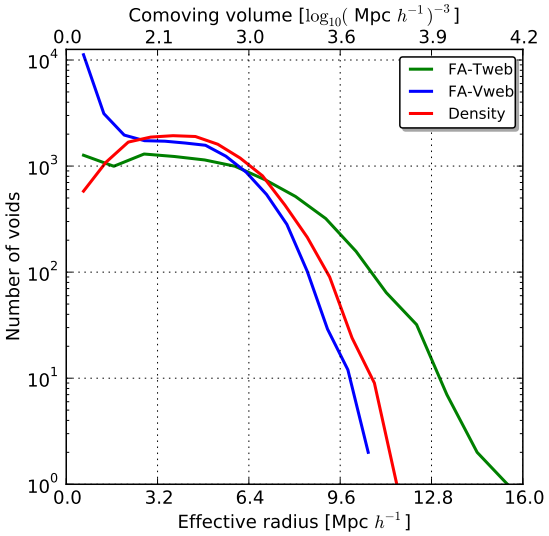

Figure 3. Volume functions of voids catalogued by each used scheme. Left panel (watershed transform over the FA field of the T-web scheme). Central panel (over the FA field of the V-web scheme). Right panel (over the density field). Gray curves correspond to voids without boundary removal whereas black curves are associated to voids merged through boundary removal process. Dotted lines correspond to original continuous fields, while segmented lines correspond to fields with a 1st-order median filtering and continuous lines to a 2nd-order median filtering.

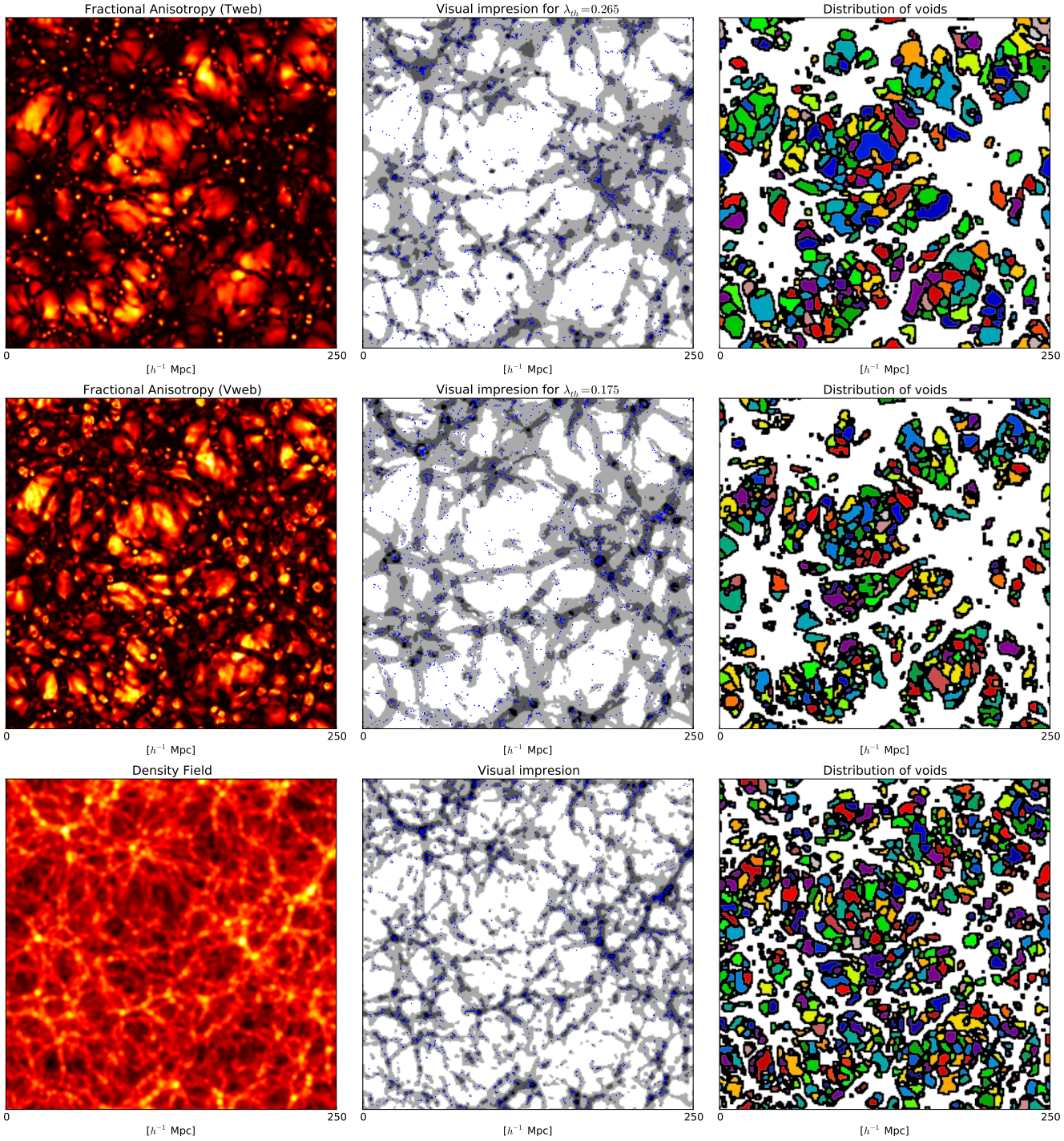

Figure 4. In left panels is shown the visual impression of the cosmic web for each web scheme (T-web, upper panels. V-web, lower panels) obtained for $\lambda_{th} = 0.0$. It can be seen each one of the defined types of environment, where voids corresponds to white zones, sheets to gray, filaments to dark gray and finally knots to black regions. In the right panels is shown the fractional anisotropy field for the same slide of the simulation and for each web schemes, where black regions correspond to FA= 1 and white regions to FA= 0. It can be noticed the degeneration of low values of FA for knots and central regions of voids, while high values of FA (FA $\lesssim 1$) are consistent with filaments and highly planar sheets. Thin dark red curves correspond to contours of $FA = 0.95$, which is approximately the transitional FA between voids and other cosmological regions.

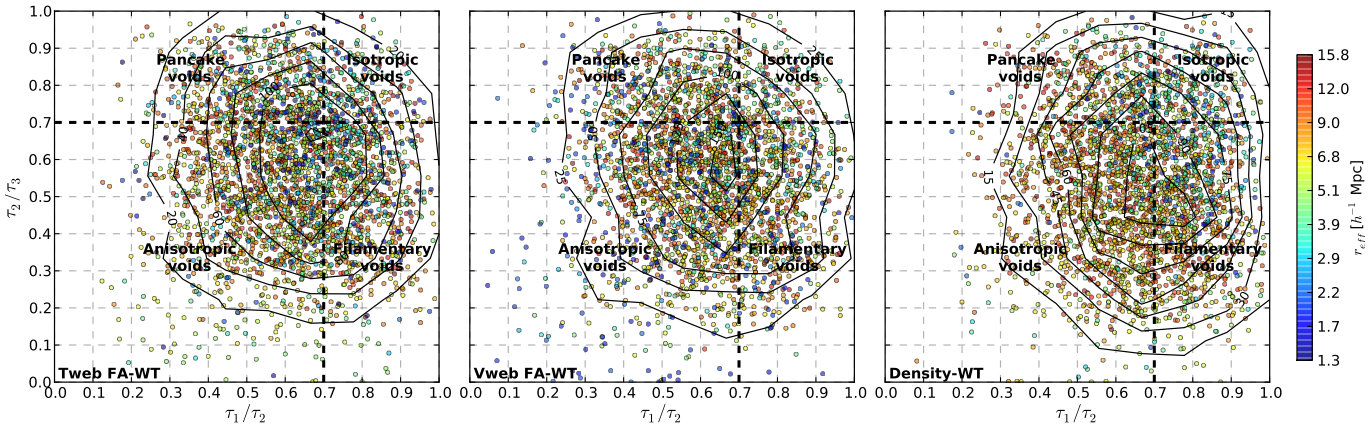

Figure 5. Volume functions of voids catalogued by each used scheme. Left panel (watershed transform over the FA field of the T-web scheme). Central panel (over the FA field of the V-web scheme). Right panel (over the density field). Gray curves correspond to voids without boundary removal whereas black curves are associated to voids merged through boundary removal process. Dotted lines correspond to original continuous fields, while segmented lines correspond to fields with a 1st-order median filtering and continuous lines to a 2nd-order median filtering.